Hydrodynamics of resonance oscillations of columns of inelastic particles

A. Goldshtein, A. Alexeev, and M. Shapiro
Laboratory of Transport Processes in Porous Materials, Faculty of Mechanical Engineering, Technion, Haifa 32000, Israel
(Received 9 February 1999)

We study oscillations of a one-dimensional (1D) column of N slightly inelastic particles, produced by a piston vibrating at one end of a closed tube. It is found that for large enough vibrational amplitudes of the piston, the column oscillates periodically with the period equal to the vibrational period. The oscillation patterns are governed by the shock waves propagating across the column. The averaged kinetic energy per particle is shown to be proportional to the square of the vibrational frequency, ω. This energy also strongly depends on the vibrational amplitude. The maximal value of this kinetic energy achievable by these external vibrations is found to be of order $\omega^2 L^2$, where L is the total volume (length) of the tube free of particles. The above results on the column resonance oscillations are also predicted by a 3D hydrodynamic model of an inelastic granular gas. [S1063-651X(99)09506-9]

PACS number(s): 83.70.Fn, 45.05.+x

I. INTRODUCTION

Hydrodynamic models of inelastically colliding particles has become a subject of growing research activity, motivated by renewed interest in granular materials [1]. Experiments show [2] that under the action of external vibrations granular materials may flow like liquids; hence it is natural to use hydrodynamic models for the description of such flows. The fluidized (gaslike) hydrodynamic granular state can be achieved only if an external source, e.g., vibrations, provides an energy input compensating the kinetic energy dissipation due to particle inelastic collisions. Without such an energy input the kinetic energy decays and, eventually, inelastic collapse occurs [3].

This paper is devoted to fluidization of layers of granular materials by external vibrations. From the hydrodynamic point of view, kinetic energy can be transferred from a vibrating plate to a granular material by ''heat flux'' and wave propagation mechanisms. The heat flux mechanism [4] prevails when the mean free path λ of the moving granules exceeds the vibrational amplitude A. The applicability of this mechanism for vibrofluidization was verified for one-dimensional [5] and two-dimensional granular systems [6,7]. Computer simulations [5,6] and experimental data [7] showed that the hydrodynamic model of Haff [4] based on this mechanism breaks down (because the majority of particles forms a slowly moving cluster), unless the system is very dilute and consists of almost elastic granules [6]. Here we discuss the wave mechanism, prevailing for $A \gg \lambda$, and show that it allows the fluidization of more dissipative granular systems than does the heat flux mechanism.

Previous studies on the wavy motion of granular materials were concerned with semi-infinite granular layers [8], or systems affected by the gravity force [9]. The results of the latter studies cannot be compared with those obtained for finite layers and without gravity [5–7]. We compare the two fluidizing mechanisms acting in a granular gas agitated by a vibrating piston in the absence of gravitation. We start our consideration from the formulation of the resonance problem for granular gas.

II. HYDRODYNAMIC MODEL

The resonance oscillations had been described for the molecular (conservative) gases [10]. Consider a gas moving within a closed tube of length L as a result of harmonic oscillations of one of its edge walls (piston). The hydrodynamic gas velocity u and the piston velocity $\dot{x}_p$ are given in this case by

$$u(L,t)=0, \quad u(x_p(t),t)=\dot{x}_p(t), \quad x_p(t)=A\sin(2\pi f t), \tag{1}$$

where A and f are the oscillation amplitude and frequency, respectively. If f is far from a certain resonance frequency, f_r (see below), the piston produces standing waves. When f is close to f_r, i.e., $|1-f_r/f| \ll 1$, the gas oscillations are amplified and shock waves develop. They travel along the tube between the piston and the resting plug with a constant speed of sound a_0 related to f_r by

$$f_r = a_0/(2L). \tag{2}$$

A space-time diagram for the first resonance is presented in Fig. 1(a). One can see that at any moment a single shock wave prevails. This wave travels with a constant speed in either direction and strikes the plug and piston once per vibrational period. Another resonance pattern may be obtained if we take the frequency f twice as large as the resonance frequency f_r [see Fig. 1(b)]. In this case two shock waves prevail at any moment. Each of these waves interacts with the plug and piston once per two vibrational periods.

The first and second resonance oscillations were experimentally registered and theoretically investigated [10] for the case of small vibrational amplitudes only. In this case the distance between the plug and piston changes insignificantly during one period, any periodic shock wave travels the same way to and fro, and can interact with the piston not more than once per period. This is, obviously, no longer true if the vibrational amplitude is of the order of the tube length L. For large enough vibrational amplitudes the distance between the

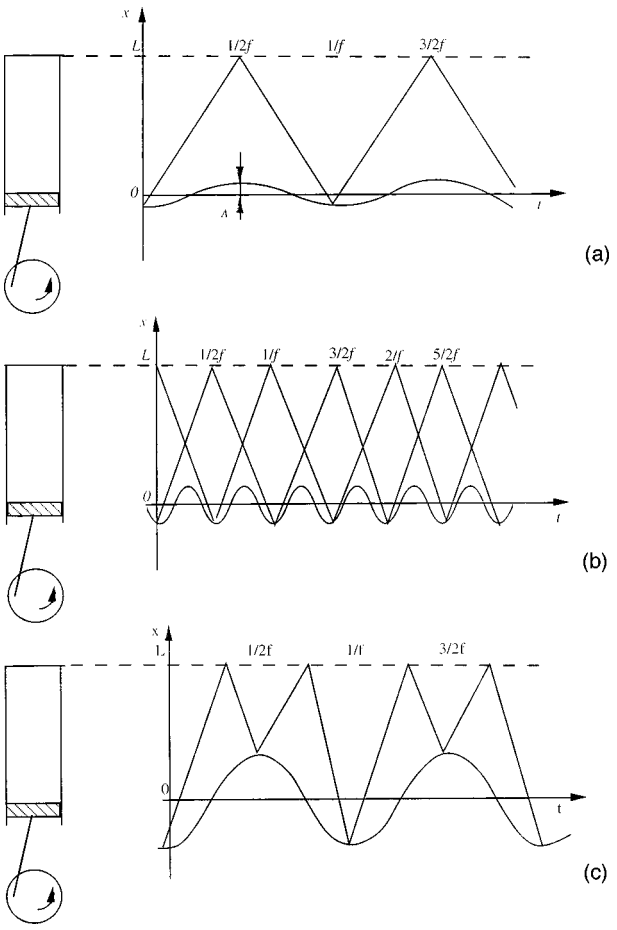

FIG. 1. Schematic of patterns of gas resonance oscillations in a closed tube: wavy line, piston path; zigzag line, shock wave path. (a) First resonance ($f=f_r$, $A\ll L$), (b) second resonance ($f=2f_r$, $A\ll L$), (c) half resonance ($f=f_r$, $A\sim L$).

plug and piston, when the latter attains the in-stroke position, can be small and additional interactions between the piston and the shock wave may take place. A schematic of such a pattern is depicted in Fig. 1(c). By the analogy with the first and second resonances, when a shock wave interacts with a piston, respectively, once per period and per two periods, we will call the pattern depicted in Fig. 1(c) the half resonance pattern. Below, we show (see Fig. 3) that the same patterns prevail also for a 1D discrete model of granular columns, when they are driven by periodic large-amplitude oscillations.

For typical laboratory conditions [10] the energy dissipated due to the gas shear viscosity and heat conduction is small compared with the energy dissipated by the shock waves. The problem of resonance oscillation of a conservative gas could thus be solved using the Euler inviscid hydrodynamic equations by series expansion in terms of small parameter $\delta=\sqrt{A/L}$ [10]. The solution shows that although the gas velocity remains small [of order $O(\delta)$], it is much larger than the piston velocity [which is of order $O(\delta^2)$]; yet both are much smaller than the speed of sound [which is of order $O(1)$].

Here we generalize this solution to the case of resonance oscillations of a dilute granular gas consisting of smooth inelastic identical spheres of diameter σ and restitution coefficient $e<1$. The Euler-type equations for this gas may be written in the form [11,12]

$$\partial_t\rho=-\partial_x(\rho u),\quad \rho(\partial_t u+u\partial_x u)=-\partial_x P,$$
$$\partial_t P+u\partial_x P+\gamma P\partial_x u=-C_0(e)\sigma^2\rho^2E^{3/2}, \tag{3}$$

where ρ is the particle number density, u is the hydrodynamic velocity, E is the average energy of particle random motion, $P=(\gamma-1)\rho E=\rho a^2/\gamma$ is the hydrostatic granular pressure for the dilute granular gas, $\gamma=\frac{5}{3}$, and C_0 is given by

$$C_0(e)=(3\pi/8)^{1/2}(1-e^2). \tag{4}$$

When $e=1$, Eqs. (3) reduce to the classical Euler equations for an ideal gas. With $e<1$, the sink term, appearing in the energy balance equation, describes the kinetic energy losses.

The above problem (1) and (3) can be solved analytically in a way similar to the solution of the classical gas problem [10], to obtain a time-periodic solution for the granular gas. Rather than doing this, here we only derive a resonance oscillation condition for the granular gas. Assuming the particle density ρ and energy E to be close to their initial constant values ρ_0 and E_0 [10], respectively, one can express (up to the leading-order term) the energy dissipation rate per unit area of the tube via the sink term as $C_0(e)L\sigma^2\rho_0^2E_0^{3/2}$. In the time-periodic regime these losses are balanced by the energy transmitted to the gas by the oscillating piston. For dilute particle systems, inelasticity affects neither conditions at the shock front nor the speed of sound [12]. Thus, the time-averaged power per unit area generated by the piston may be taken from the solution for conservative gases in the form [10]

$$E_p=-\frac{1}{T}\int_0^T Pu_{x=L}dt=\frac{16}{3\sqrt{\gamma+1}}\rho_0a_0^3\left(\frac{A}{L}\right)^{3/2}.$$

Equating the expressions for energy generation and dissipation, we get the necessary condition for resonance oscillations of a nonconservative granular gas:

$$\delta^3=(A/L)^{3/2}=0.284(1-e^2)N, \tag{5}$$

where $N=L\rho_0\sigma^2$ is the number of particles in the volume $L\sigma^2$. For e close to unity the right-hand side of Eq. (5) is close to the parameter $N(1-e)/2$ used in [5,13] as a characteristic of the dissipative properties of granular systems. According to Eq. (5) the total energy generation is of the order δ^3, which is consistent with the weak shock wave approximation (see [10]) implicitly employed in the solution.

It should be noted that the resonance oscillations in the classical and inelastic gases have different physical origins. In the classical gas the resonance is due to the proximity of the piston's frequency to the inherent system's frequency f_r, determined by its temperature (speed of sound). In contrast,

in the granular gas the resonance oscillations occur when a balance exists between the inelastic dissipation and production of granular kinetic energy due to the piston's power, which is equal to the shock wave production power [10].

Condition (5) implies that for a fixed energy dissipation the resonance occurs only for large enough amplitudes δ predicted by Eq. (5). Since $\delta<1$, condition (5) predicts also the maximal energy dissipation (which is formally obtained by setting $\delta=1$). It is remarkable that in contrast to the conservative gases, the resonance condition for the granular gas is independent of the vibrational frequency f and the initial kinetic energy E_0. It means that f and L define a_0 through relation (2). Therefore, any vibrational frequency will be the resonance one, since any initial state with an arbitrary kinetic energy E_a will eventually evolve to the resonance state [14], where the dissipated and generated amounts of energy are balanced. In this state the speed of sound and the kinetic energy in the system are given by

$$a_r=2Lf, \quad E_r=a_r^2/\gamma(\gamma-1). \tag{6}$$

III. COMPUTER SIMULATION

Equations (5) and (6) are, strictly speaking, applicable when $\delta\ll 1$, which implies that the energy dissipation parameter $D\equiv N(1-e)\ll 1$. However, we show that the resonance oscillations may be generated for more dissipative granular systems. To demonstrate this we present the results of computer simulations of the motion of N sizeless inelastic particles with identical masses constrained to move along a line between a harmonically oscillating piston and a resting plug, in accordance with boundary conditions (1). The particles are enumerated in the direction from the piston to the plug. The boundaries collide with the first and Nth particle in an elastic manner.

We aim at comparing the results of simulations with the predictions of the hydrodynamic model and the results of similar calculations of [5] performed for the heat flux energy transfer mechanism. Towards this goal we used the collisional models of hard [4] and soft [15] inelastic particles.

A. Hard-sphere model

We start our considerations with the hard-sphere collisional model. The results of the simulations presented were obtained by a driven-event method [5,6,16] and for the dissipation parameter $D\leqslant 1$. We consider two physical situations where A is, respectively, less and larger than $\lambda=L/N$, thereby distinguishing between these regimes and the corresponding energy transfer mechanisms.

In the initial state treated, the particles were uniformly distributed with velocities randomly chosen between $-\sqrt{2E_a}$ and $\sqrt{2E_a}$, where $E_a\gg E_r$, given by Eqs. (6). The average kinetic energy per particle per second, $\overline{E}(t)$, was used to characterize the system's state. We found that after some time this energy converges to a constant amount $\overline{E}^{\infty}$ which slightly depends on E_a. $\overline{E}^{\infty}$ was found to be proportional to f^2, in accordance with the dimensionality arguments [see the discussion preceding Eq. (6)]. Hence, it is convenient to scale all system's parameters with the tube length and the vibrational frequency, and to take A as the only characteristic of the boundary conditions. (Thus, the dimensionless tube length and vibrational period are both equal to unity.) To characterize the system's ability to dissipate kinetic energy, we did simulations with various N and $1-e\ll 1$ for constant $D=N(1-e)$, and did not find any significant difference in $\overline{E}^{\infty}$. As such, any system's state is uniquely characterized in terms of A and D [cf. condition (5)], i.e., $\overline{E}^{\infty}=\overline{E}^{\infty}(A,D)$. Figure 2 presents $\overline{E}^{\infty}$ versus the dimensionless vibrational amplitude for several $D\leqslant 1$. Each curve has several global and many local maxima. Our simulations show that the local maxima in Fig. 2 are caused by the effect of initial conditions, whereas the global maxima are practically independent of these conditions. In the present paper we focus on the global maxima which are associated with different patterns of the system motion (see below), and leave investigation of the local maxima for future contributions.

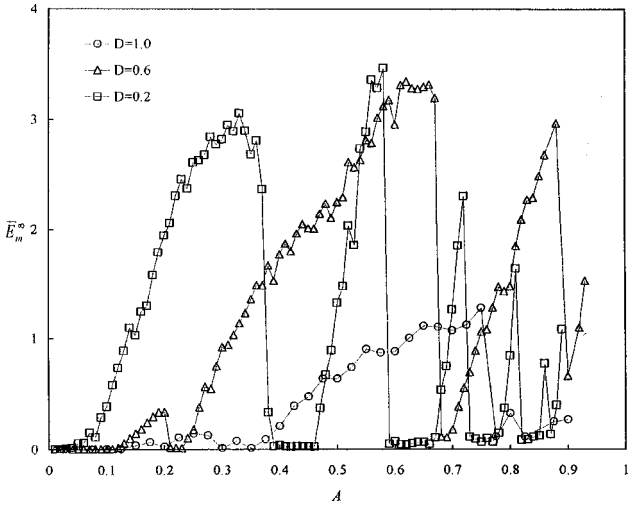

FIG. 2. Kinetic energy vs vibrational amplitude for $N=100$.

Figures 3(a)–3(c) present three examples of the particles' trajectories during two vibrational periods, corresponding to the three global maxima of the function $\overline{E}^{\infty}(A,0.6)$. When $A\sim 0.2$, five groups of particles (clusters) oscillate with period T_2 close to 2 [Fig. 3(a)]. We will call this pattern, by the analogy with pattern depicted in Fig. 1(b), the second resonance pattern (see below for a discussion of this notion). One of the clusters (close to the plug) moves with a small amplitude, whereas four others oscillate with large amplitudes of about $\frac{1}{2}$. Note that the center of mass of the column oscillates almost periodically around an equilibrium position $x_e\sim\frac{3}{4}$ with the amplitude much smaller than those of the four clusters. x_e is governed by the number of slowly moving particles, which is much larger than the number N_m of rapidly moving ones (see below Fig. 6). Generally, the initial conditions affect the number of clusters, but not T_2 and N_m.

Figure 3(b) shows two groups of particles corresponding to the second maximum $(A=0.66)$, oscillating with period 1 but with different amplitudes. The center of mass oscillates with a larger amplitude (about $\frac{1}{2}$). The fast moving cluster hits the piston once per period. This is called here, by the analogy with the pattern depicted in Fig. 1(a), the first resonance pattern.

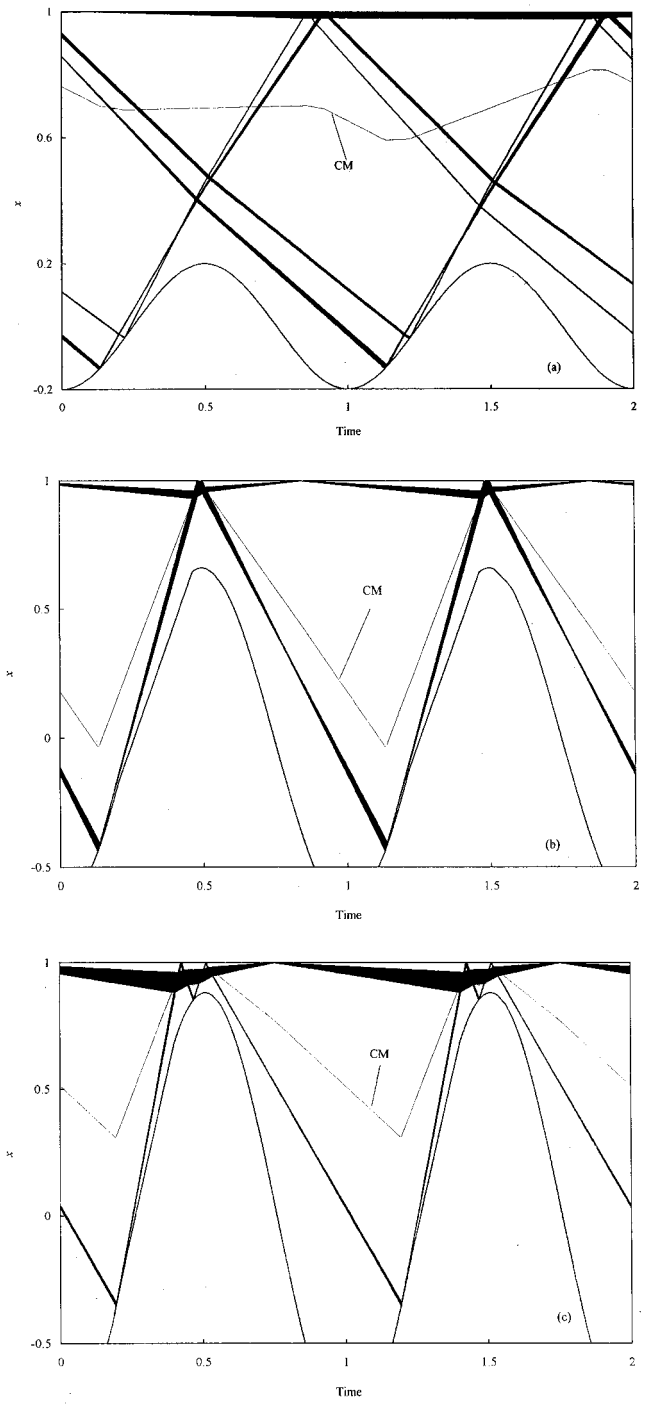

FIG. 3. Trajectories of particles' resonance oscillations ($D=0.6$, $N=100$). Piston moves sinusoidally—$A\sin 2\pi t$: (a) second resonance pattern ($A=0.2$), (b) first resonance pattern ($A=0.66$), and (c) half resonance pattern ($A=0.88$); CM, position of center of mass.

For $A>0.86$, particle clusters oscillate in a different manner. Figure 3(c) shows a two-cluster pattern, which differs from the first resonance pattern. The faster cluster hits the piston twice per period. We call this the half resonance pattern by analogy with Fig. 1(c).

Decreasing D leads to patterns with three, four, etc., collisions per period between the fast cluster and the piston. For $D=0.2$, patterns with three and four collisions appear for $A=0.7$ and 0.8, which values correspond to the maxima of

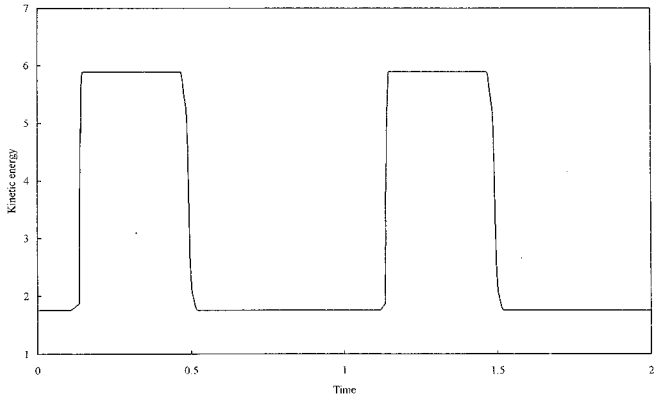

FIG. 4. Kinetic energy vs time for $A=0.66$, $D=0.6$, $N=100$.

$\overline{E}^{\infty}(A,0.2)$ (see Fig. 2). With D increasing from 0.6 to 1.0, patterns with multiple cluster-plug collisions disappear. However, additional (with respect to the case $D=0.6$) global maxima of $\overline{E}^{\infty}(A,1.0)$ emerge, corresponding to the particles' oscillations with periods 3 (third resonance, $A=0.25$), 4 (fourth resonance, $A=0.18$), etc. For all such maxima we registered that the smaller the amplitude A at the maximum, the smaller N_m and the larger the oscillation period.

It is noteworthy that the maximal kinetic energy $\overline{E}^{\infty}$ that can be pumped into the system by the vibrational excitation only slightly depends on the energy dissipation (as expressed by D) for small and moderate D. In Fig. 2 we find that $\overline{E}^{\infty}_m(0.2)\approx 3.6$ and $\overline{E}^{\infty}_m(0.6)\approx 3.7$. These values are both close to the prediction of the hydrodynamic model. Indeed, rewriting Eq. (6) in a dimensionless form (by setting $f=1$ and $L=1$) and setting $\gamma=\frac{5}{3}$, for smooth inelastic spheres, one gets $E_r\sim 3.6$. In spite of the difference between the simulated 1D granular system and the 3D granular gas model given by Eqs. (3), the hydrodynamic estimation of $\overline{E}^{\infty}_m$ agrees with the DEM simulations.

This agreement between the computational and hydrodynamic models may look like a coincidence. Below we show that the analogy between these models is much deeper than it might seem, and the processes of generation and dissipation of kinetic energy for both systems are governed by the shock waves. In order to get insight into these processes, we plotted the current dimensionless kinetic energy versus time in Fig. 4 for the first resonance conditions [see Fig. 3(b)]. One can see that there are two very brief periods of time during which the energy changes dramatically. These rapid changes of the energy are associated with interactions of the first group of the particles with the piston and the second group of the particles, respectively. During the interactions with the piston the system gains kinetic energy and during the interaction between these two groups the system loses its energy. During the time between these interactions the energy changes insignificantly. It means that interpartical collisions occur during very small portions of the vibrational period. Therefore, for the time scale chosen each interaction looks like a jump of the kinetic energy.

In order to get insight into the piston-particle interaction, we depict velocity distributions versus particle number in Figs. 5(a)–5(c) for several moments of time within the period where the kinetic energy increases. These moments are

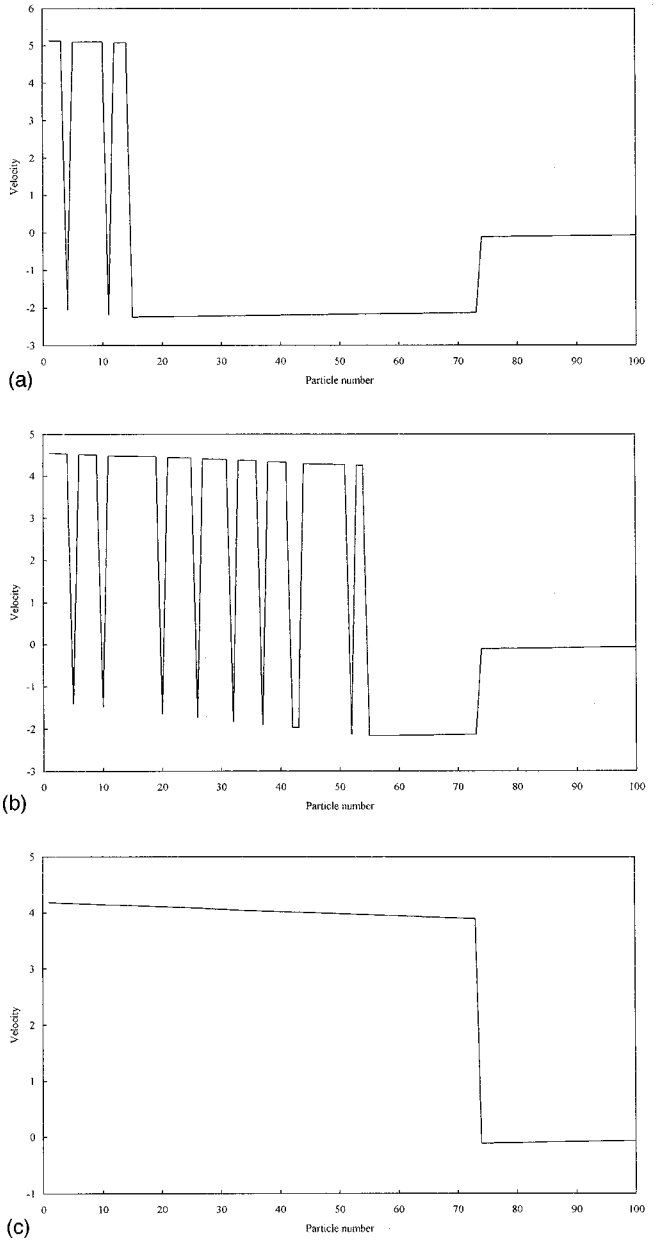

FIG. 5. Velocity distribution within granular column for $A=0.66$, $D=0.6$, $N=100$, and times τ of piston-particle interaction: (a) $\tau=0.68$, (b) $\tau=0.77$, and (c) $\tau=1.0$. The times τ are given in the portion of the piston-column contact period which in the present regime is equal to 0.042 52 of the vibrational period.

expressed as a fraction of the period of contact between the particles and the piston. Figure 5(a) corresponds to a beginning of the contact. Particles may be subdivided into three groups. The first group of the particles with numbers from 74 to 100 corresponds to the cluster slowly moving about the plug. The second group of particles with numbers from 15 to 73 moves towards the piston with velocities close to -2. Velocities of these particles are the same as they were just before the collision with the piston. The first and second groups of particles still ''do not know'' about the piston and thus constitute an undisturbed part of the column. In this undisturbed region the velocity dispersion is very small.

Particles with numbers from 1 to 14 form the third group. There is a significant dispersion in velocities within this group: some of the particles move in the positive direction, whereas others move in the negative direction. This dispersion is apparently affected by the impact with the piston. The third group constitutes the disturbed part of the column.

In Fig. 5(b) we see that at later times the disturbances propagate into the layer. The number of particles in the second group is significantly increased due to the decreasing of the particle number in the third group. The disturbances propagate from ''hot'' (large velocity dispersion) into ''cold'' gas (small velocity dispersion). In the hydrodynamic terms the process described above may be called strong shock wave propagation [17]. The boundary between the third and second groups may be identified with the shock wave front.

Due to high particle density, the disturbances propagate very quickly and all particles forming the third and second group are gradually involved in the interparticle collision process. Numerous inelastic collisions lead to rapid dissipation of the particle relative kinetic energy. As a result, after some time particles of the third and the second groups lose almost all their relative energy, and form a new group of particles moving with speeds of about 4, as seen in Fig. 5(c).

It is worth mentioning that the velocity is distributed monotonically within both groups of particles shown in Fig. 5(c). Due to such a distribution the particles avoid collisions and, hence, energy losses. That is why the velocity distribution depicted in Fig. 5(c) remains unchanged until the intergroup collision occurs. This collision has many features of particle-piston collision. The energy of the translational particle motion transforms, as a result of the shock wave propagation, into the energy of relative particle motion. This energy is dissipated through the interparticle collisions. As a result, the total energy of the column rapidly changes from about 5.8 to 1.8 (see Fig. 4).

The dimensionless kinetic energy $\overline{E^{\infty}}$ calculated for $A<0.1$ and $D>0.6$ is small compared with $\overline{E_m^{\infty}}$ and indistinguishable in Fig. 2. In order to compare $\overline{E^{\infty}}$ for different A we normalized $\overline{E^{\infty}}$ by the maximal piston velocity, as in [5,6]. This rescaled energy is found independent of A for $0.6<D<1$ and $0.01<A<0.1$ and with a good accuracy may be approximated by $0.005/D$. With this scaling the maximal kinetic energy is $\tilde{E}_m^{\infty}=\overline{E_m^{\infty}}/(2\pi A_m)^2$, where A_m is the amplitude corresponding to the maximal energy, i.e., $\overline{E_m^{\infty}}=\overline{E^{\infty}}(A_m,D)$. Using concomitant values of A_m and $\overline{E_m^{\infty}}$ from Fig. 2, one calculates $\tilde{E}_m^{\infty}=0.078$ and 0.19 for $D=0.2$ and 0.6, respectively. These are much larger than the respective values 0.003 and 0.0082, calculated from the approximation $0.005/D$, apparently corresponding to the heat flux excitation mechanism [5].

We found that for the regimes where $\overline{E_m^{\infty}}\sim 0.005/D$, N_m is small (one to three particles) and independent of A, as was also shown in [5]. When the dissipation parameter D decreases from 0.6 to 0.2, the range of amplitudes for which $\tilde{E}_m^{\infty}$ is independent of A diminishes. For example, for $D=0.2$ this range is $A<0.01$. Beyond this range an increase of $\tilde{E}_m^{\infty}$ is accompanied by growth of N_m.

The applicability of the hydrodynamic description to a particulate system depends on the kinetic energy distribution

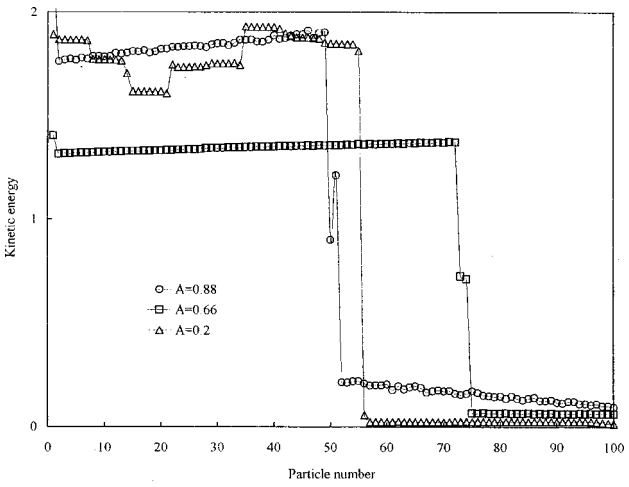

FIG. 6. Kinetic energy distribution for $D=0.6$, $N=100$.

between the particles, rather than on the total kinetic energy $\overline{E}^{\infty}$. In Fig. 6 the kinetic energy distribution for several amplitudes is presented for $D=0.6$. All curves are normalized in such a way that the area below the curve is equal to 1. The amplitudes chosen correspond to three maxima of $\overline{E}^{\infty}$ (see Fig. 2) related to three different patterns of the particles' motion (see Fig. 3), each characterized by its own N_m. The maximal of these three N_m values, namely $N_m=75$, is achieved for $A=0.66$ corresponding to the first resonance pattern. Increasing A to 0.88 (the half resonance pattern) results in decreasing N_m to 51, though the energy distribution between the rapidly and slowly moving particles changes in favor of the slow movers. The curve in Fig. 6 for $A=0.225$ demonstrates that the second resonance pattern provides a larger number of fast particles ($N_m=55$) than the half resonance, notwithstanding that the vibrational amplitude is much larger in the half resonance pattern.

We calculated the numbers N_m for other vibrational amplitudes and found that the maxima of the kinetic energy, $\overline{E}^{\infty}$, correlate with the maxima of N_m. Even a small increase of A from any of the values listed in Fig. 3 is accompanied by a dramatic decrease of both $\overline{E}^{\infty}$ (see Fig. 2) and N_m. For example, a change from $A=0.66$ to 0.68 leads to a drop in N_m from 75 to 5. Such sharp changes indicate the existence of a resonance between the degrees of freedom associated with different particles. Each of these degrees of freedom is characterized by its own A-dependent frequency. Hence, variation of A can change these frequencies for some particles, equalizing them, i.e., producing simultaneous oscillations of the particles' groups. Using such an explanation, we may call the patterns presented in Figs. 1(a)–1(c) resonance oscillations of $N_m=55$, 75, and 51 particles, respectively, out of the total of 100 particles.

B. Soft-sphere model

The hard-sphere model is mathematically the simplest one. For real materials, however, the restitution coefficient is not constant. Rather, it increases monotonically with decreasing relative velocity of colliding particles [18]. This collisional property, apparently disregarded by the hard-sphere model, can lead to significant differences in the results of simulations [19,20]. Below we reexamine the problem of resonance oscillations of a column of inelastic particles using a more physically accurate collisional model [15]. According to this model, during interparticle contact the particle compression distance $\xi_i=R_i+R_{i+1}-|x_i-x_{i+1}|$ is governed by the equation

$$\ddot{\xi}_i+\rho[\dot{\xi}_i^{3/2}+\tfrac{3}{2}A_d\dot{\xi}_i\sqrt{\xi_i}]=0, \tag{7}$$

where $i=1,2,\ldots,100$,

$$\rho=\frac{2Y\sqrt{R^{\mathrm{eff}}}}{3m^{\mathrm{eff}}(1-\nu^2)}, \quad m^{\mathrm{eff}}=\frac{m_i m_{i+1}}{m_i+m_{i+1}}, \quad R^{\mathrm{eff}}=\frac{R_i R_{i+1}}{R_i+R_{i+1}}. \tag{8}$$

Here Y is the Young modulus, ν is the Poisson ratio of the particle material, A_d is a material constant dependent on Y, ν, and the material effective bulk viscosity constant μ governs energy losses through collisions. Particle-particle and particle-wall collision are, respectively, described by setting in Eq. (8) $m^{\mathrm{eff}}=m/2$, $R^{\mathrm{eff}}=R/2$ and $m^{\mathrm{eff}}=m$, $R^{\mathrm{eff}}=R$, where m and R are the particle mass and radius, respectively. The parameter A_d, appearing in Eq. (7), accounts for the energy losses during the collision, and, hence, it is related to the effective restitution coefficient e_{eff}. For a fixed A_d, this restitution coefficient depends on the relative velocity of colliding particles.

Using the above collisional model, the equations of motion of the system may be described by the Newton second and third laws. These may be expressed by the system of $N=100$ second-order differential equations. For the numerical simulations presented below, we solved this system by the fourth-degree Runge-Kutta numerical integration scheme. The time step was chosen small enough to not affect the results of the simulations.

Simulations were performed for the following fixed values of the parameters: $m=0.057\,\mathrm{kg}$, $R=0.005\,\mathrm{m}$, $\nu=0.35$, and $Y=9.8\times10^{10}\,\mathrm{N/m^2}$. These values of the Young modulus and the Poisson ratio correspond to the real material—brass. In order to mimic results of the hard-sphere simulations, the following values of A_d were used: $A_d\times10^8=1.04$, 3.14, and 5.25. These values correspond to the effective restitution coefficients $e_{\mathrm{eff}}=0.99$, 0.994, and 0.998 calculated for the two particles colliding with relative velocity equal to $\sqrt{2E_r}\approx2.68$. Here E_r is the dimensionless resonance energy [see Eq. (6)] calculated for the first resonance.

The hard-sphere simulations were performed for sizeless particles which apparently do not occupy any volume (length) within the 1D tube. For the soft-sphere simulations particles have a certain size. In order to compare the results of the simulations obtained by both collisional models, for the soft collisional model simulations the total volume (length) free from the particles within the tube was taken to be equal to the tube length, L, for the hard-sphere collisional model simulations.

For the parameters chosen we repeated all simulations performed for the hard-sphere model and observed the trends

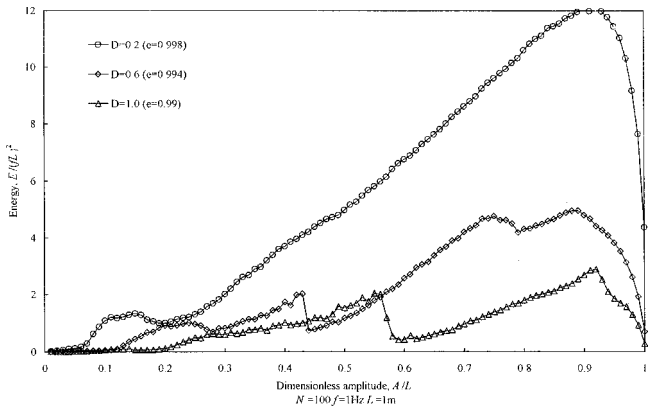

FIG. 7. Kinetic energy vs vibrational amplitude for a column of $N=100$ softly colliding granules.

reported above. In particular, we found that the time-averaged kinetic energy approaches a constant value $\overline{E}^{\infty}$ which depends on the two dimensionless parameters: vibrational amplitude A and dissipative parameter $D=N(1-e_{\mathrm{eff}})$. In Fig. 7, $\overline{E}^{\infty}$ is shown versus the dimensionless vibrational amplitude for several $D\leqslant 1$. Each curve has several global maxima. As for the hard-sphere model, each of these global maxima is associated with a resonance pattern. Examples of these resonance patterns are presented in Figs. 8(a)–8(d). Comparing these patterns with those depicted in Fig. 3, one can see that they may be classified as the first [Figs. 8(a) and 8(b)] and half [Figs. 8(c) and 8(d)] resonance patterns. The second resonance pattern was not observed for the soft-sphere model simulations.

The nature of the velocity-dependent restitution coefficient manifests itself in the disappearance of the clusters observed for the hard-sphere model. In contrast to the latter model, now trajectories of each particle are well distinguished. They fill practically all the phase volume in the plane x-t. The period of contact between the piston and column significantly increases, and reaches half of the vibrational period. In order to get qualitative information about the processes occurring within the column, we plotted in Fig. 9 the kinetic energy evolution [Fig. 9(a)] and the particles' and piston's trajectories [Fig. 9(b)], respectively, during one vibrational period. One can distinguish in Figs. 9(a) and 9(b) several characteristic stages of the system evolution. The moments of time separating these stages are denoted by *a*,*b*,*c*. At the moment *a* the kinetic energy reaches its minimum [see Fig. 9(a)] and the piston approaches its outstroke position [see Fig. 9(b)]. At the moment *b* the column detaches from the piston [see Fig. 9(b)] and the energy reaches its maximum [see Fig. 9(a)]. At the moment *c* the column again touches the piston moving to the outstroke position.

Velocity distributions within the column for the moments *a*,*b*,*c* are depicted in Figs. 10(a)–10(c), respectively. One can distinguish in Fig. 10(a) a shock wave pattern. About 20 first particles are involved in intensive relative motion by the shock wave generated by the piston. The rest of the particles are less agitated because the wave front has not yet reached them. During the stage, between the moments *a* and *b*, the piston, moving in the positive direction, pushes the shock wave towards the plug. This shock wave compresses the column of particles and increases their energy from 1.5 to 7 [see Fig. 9(a)]. We see in Fig. 10(b) that the whole layer is in-

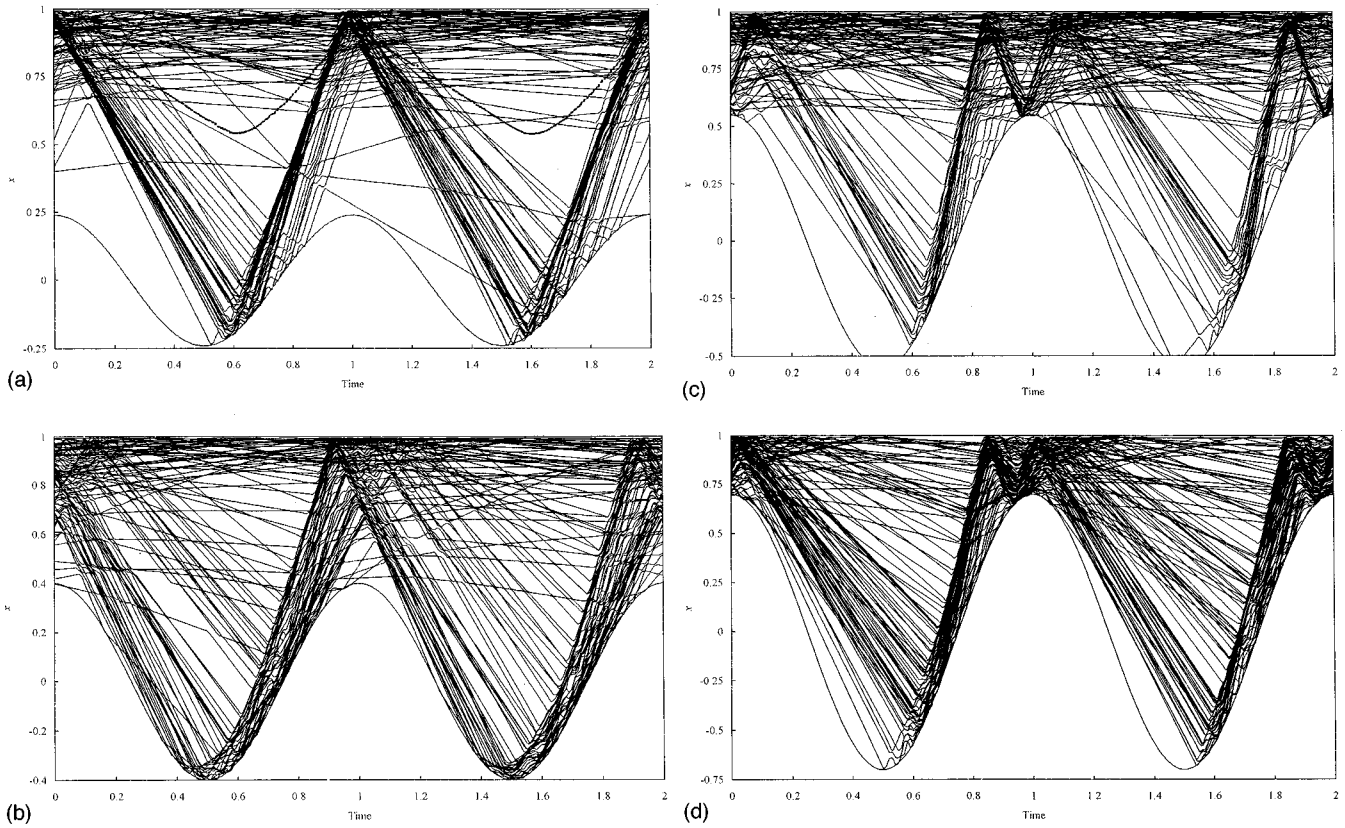

FIG. 8. Patterns of particles' resonance oscillations (soft collisional model, $D=0.6$, $N=100$). Piston moves sinusoidally—$A\sin 2\pi t$: (a) $A=0.24$, (b) $A=0.4$, (c) $A=0.55$, and (d) $A=0.7$. (a) and (b) First resonance pattern; (c) and (d) half resonance pattern.

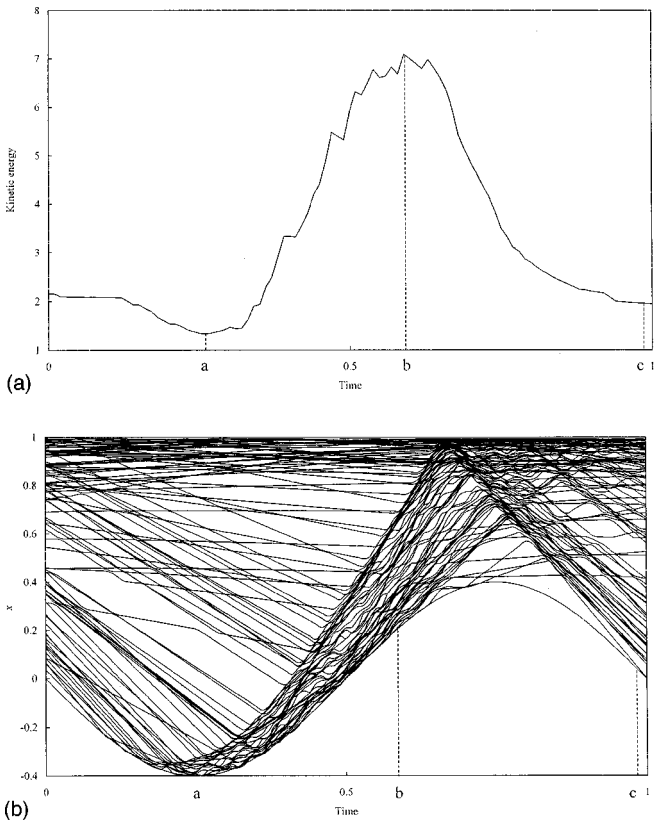

FIG. 9. Evolution of a column consisting of $N=100$ inelastically colliding (soft collisional model) granules during one vibrational period for $A=0.66$, $D=0.6$. (a) Kinetic energy vs time, and (b) particles and piston trajectories.

volved in the intensive relative (thermal) motion at the end of this stage. All particles move in the positive direction, except the last particle, which is reflected from the plug. There is a significant dispersion in velocities between the particles, i.e., they are all fluidized.

During the detachment period lasting until the moment c, the particles rapidly lose their energy [see Fig. 9(a)]. It is explained by the absence of interaction with the piston, which does not supply energy to the column. The energy losses are caused by a vast number of inelastic collisions stipulated by significant dispersion of the particles' velocities. These collisions are accompanied by rather complicated wavy processes. Any detailed description of these processes is far beyond the scope of the present paper and may be a subject of a separate investigation. It is worth mentioning that this stage terminates when an expansion wave is formed. An example of this wave is presented in Fig. 10(c). The total momentum of the column is negative (most of the particles move towards the piston), though the relative particle velocities are still significant. A part of the kinetic energy of the relative particle motion is lost through inelastic collisions. The remaining part is distributed between the particles, in such a way that a velocity gradient is created. Such a gradient may be seen in Fig. 10(c) within the part of the column counting about the first 80 particles. Comparing the velocity distributions of the last 80 particles presented in Figs. 10(a) and 10(c), we see that the intensive particle thermal motion terminates and the velocity distribution transforms into an almost monotonic one during the time period $(0,a)$. Due to such velocity distribution, caused by the expansion wave, the column expands. After that, a new shock wave compresses the column and the process repeats again.

The results presented above of our computer simulations of vibrated inelastic granular columns, performed for both collisional models, have many common features, as follows.

(i) For large enough vibrational amplitudes of the piston the columns oscillate periodically with a period equal to the vibrational period.

(ii) The maximal value of the kinetic energy of these granular systems driven by the external vibrations is proportional to the square of the vibrational frequency, ω, and strongly depends on the vibrational amplitude in a nonmonotonic manner. The maximal values of the kinetic energy, achievable by means of external vibrations, are of the order of $\omega^2 L^2$, where L is the total volume of the space within the tube free of particles.

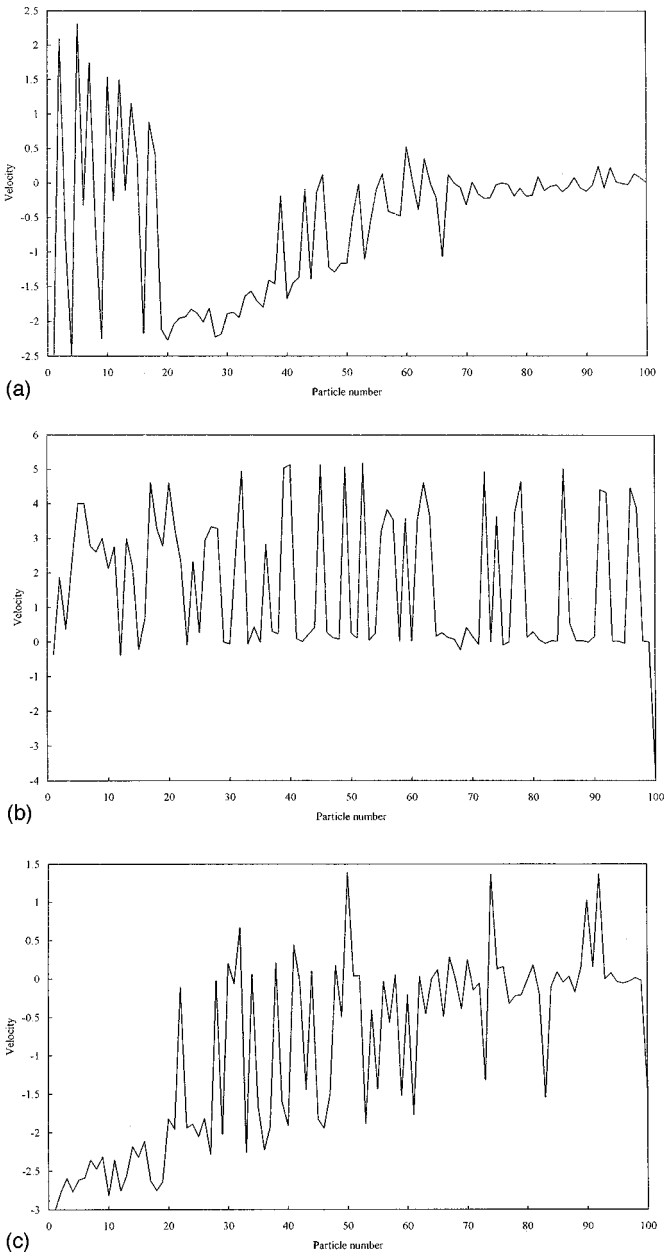

FIG. 10. Particle velocity distribution within the column shown in the Fig. 9: (a) $t=a$, (b) $t=b$, and (c) $t=c$.

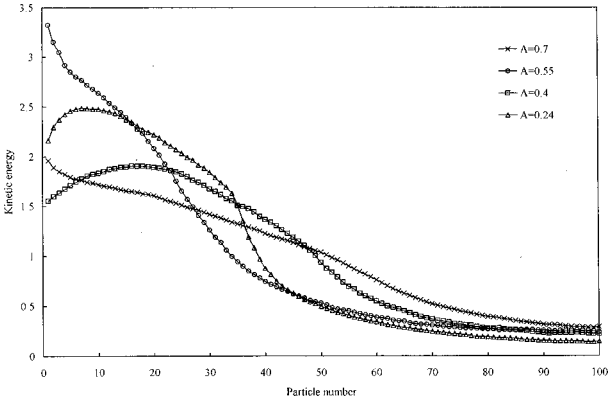

FIG. 11. Kinetic energy distribution for $D=0.6$, $N=100$.

(iii) The periodic oscillations of the granular columns corresponding to the maximal values of the kinetic energy are governed by the shock waves. All the features (i)–(iii) listed above were shown in Sec. II to prevail for resonance oscillations also of three-dimensional granular gases, as predicted by the hydrodynamic model of the granular gas (1) and (2). Moreover, prediction of the maximal value of the kinetic energy (6) calculated on the basis of the developed hydrodynamic model is in good agreement with the computer simulation results for the hard-sphere model.

We also registered a number of differences in the results of soft- and hard-sphere model simulations. In particular, periods of piston-particle interactions for ''soft'' particles are considerably larger than those for ''hard'' ones. Another important difference between these collisional models is in the energy distribution between the particles. In Fig. 11 the kinetic energy distribution for several amplitudes is presented for $D=0.6$. All curves are normalized in such a way that the area below the curve is equal to 1. The amplitudes chosen correspond to four maxima of $\overline{E^{\infty}}$ for $D=0.6$ (see Fig. 7) related to the two different patterns of particle motion (namely, first resonance [Figs. 8(a) and 8(b)] and half resonance [Figs. 8(c) and 8(d)]). Comparing velocity distributions obtained for the soft- (Fig. 11) and hard- (Fig. 6) sphere collisional models, one can see that the jumps of the energy between two groups of particles, registered for the hard-sphere model, do not exist for the soft collisional model. In that sense the energy distribution of the vibrated 1D granular columns calculated for the soft collisional model matches closer to the comparable property of the resonance oscillations of the granular gases based on the continuum approach than do the results for the hard-sphere model. On the other hand, we have seen above that the maximal value of the kinetic energy predicted by the hydrodynamic model matches closer to the results of the hard-sphere model simulations.

These resonance oscillations of our 1D system have several common features with those described by the hydrodynamic model, discussed above. A more detailed comparison between the models and the simulations is hardly possible because of the following two reasons. The hydrodynamic model is restricted by the requirement of the smallness of the vibrational amplitude. Therefore, significant errors may arise in the description of the column oscillations under the action of large amplitude external excitations considered in our 1D simulations. In particular, the hydrodynamic model fails to treat the half resonance pattern corresponding to multiple reflections of the shock wave from the walls, when the distance separating them becomes small enough. The second reason is the physical difference between a 1D system and 2D and 3D systems. It is known [21] that even the 1D column of elastically colliding spheres oscillates in a manner different from that of the comparable 3D conservative gas. We hope that future comparison of CFD simulations with 2D and 3D physical and computational experiments will allow us to assess the applicability of these and similar hydrodynamic models to vibrated granular systems.

ACKNOWLEDGMENTS

This research was supported by the Israel Science Foundation, by the Center of Absorption in Science, and the Gilliady Program for Immigrant Scientists Absorption by the Fund for the Promotion of Research at the Technion.

[1] I. Gutman, *Industrial Uses of Mechanical Vibrations* (Business Books, London, 1968); B. J. Ennis, in *Proceedings of the Third International Conference on Powders and Grains, Durham, 1997*, edited by R. P. Behringer and J. T. Jenkins (A. A. Balkema Publishers, Rotterdam, 1997), pp. 13–23.

[2] H. M. Jaeger, S. R. Nagel, and R. P. Behringer, Rev. Mod. Phys. **68**, 1259 (1996), and references therein.

[3] I. Goldhirsch and G. Zanetti, Phys. Rev. Lett. **70**, 1619 (1993).

[4] P. K. Haff, J. Fluid Mech. **134**, 401 (1983).

[5] Y. Du, H. Li, and L. P. Kadanoff, Phys. Rev. Lett. **74**, 1268 (1995).

[6] E. L. Grossman, T. Zhou, and E. Ben-Naim, Phys. Rev. E **55**, 4200 (1996); S. McNamara and J. L. Barrat, *ibid.* **55**, 7767 (1997).

[7] A. Kudrolli, M. Volpert, and J. P. Gollub, Phys. Rev. Lett. **78**, 1383 (1996).

[8] A. Goldshtein, M. Shapiro, and C. Gutfinger, J. Fluid. Mech. **316**, 29 (1996); **327**, 117 (1996).

[9] A. Goldshtein, M. Shapiro, L. Moldavsky, and M. J. Fichman, J. Fluid Mech. **287**, 349 (1995); A. V. Potapov and C. Campbell, Phys. Rev. Lett. **77**, 4760 (1996).

[10] B. Betchov, Phys. Fluids **1**, 205 (1958); W. Chester, J. Fluid Mech. **18**, 44 (1964); A. Goldshtein, P. Vainshtein, M. Fichman, and C. Gutfinger, *ibid.* **322**, 147 (1996).

[11] C. K. K. Lun, S. B. Savage, D. J. Jeffery, and N. Chepurniy, J. Fluid Mech. **140**, 223 (1984); J. T. Jenkins and M. W. Richman, Arch. Ration. Mech. Anal. **87**, 355 (1985).

[12] A. Goldshtein and M. Shapiro, J. Fluid Mech. **282**, 75 (1995).

[13] B. Bernu and R. Mazighi, J. Phys. A **23**, 5745 (1990).

[14] It is true for $E_a > E_r$. For $E_a \ll E_r$, the granular gas never comes to the resonance state. V. Kamenetsky, A. Goldshtein, M. Shapiro, and D. Degani (unpublished).

[15] N. V. Brilliantov, F. Spahn, J.-M. Hertzsch, and T. Pöschel, Phys. Rev. E **53**, 5382 (1996).

[16] S. McNamara and W. R. Young, Phys. Fluids A **4**, 496 (1992); S. Luding, E. Clement, A. Blumen, J. Rajchenbach, and J. Duran, Phys. Rev. E **49**, 1634 (1994).

[17] Ya. B. Zel'dovich and Yu, P. Raizer, *Physics of Shock Waves and High-temperature Hydrodynamic Phenomena* (Academic, New York, 1967).

[18] W. Goldsmith, *Impact* (Edward Arnold Ltd., London, 1960).

[19] F. Spahn, U. Schwarz, and J. Kurths, Phys. Rev. Lett. **78**, 1596(1997).

[20] D. Godman, M. D. Shattuck, C. Bison, W. D. McCormick, and Harry L. Swinney, Phys. Rev. E **57**, 4831 (1998).

[21] A. J. Lichtenberg and M. A. Lieberman, *Regular and Stochastic Motion* (Springer-Verlag, New York, 1983).